OXFORD

GENERAL ARTICLE

LRP2 controls sonic hedgehog-dependent differentiation of cardiac progenitor cells during outflow tract formation

Annabel Christ[*,†], Maike Marczenke and Thomas E. Willnow

Max-Delbrueck-Center for Molecular Medicine, 13125 Berlin, Germany

[*]To whom correspondence should be addressed at: Max-Delbrueck-Center for Molecular Medicine, Robert-Roessle-Str. 10, D-13125 Berlin, Germany. Tel: +49-30-9406-3747; E-mail: annabel.christ@mdc-berlin.de

Abstract

Conotruncal malformations are a major cause of congenital heart defects in newborn infants. Recently, genetic screens in humans and in mouse models have identified mutations in *LRP2*, a multi-ligand receptor, as a novel cause of a common arterial trunk, a severe form of outflow tract (OFT) defect. Yet, the underlying mechanism why the morphogen receptor LRP2 is essential for OFT development remained unexplained. Studying LRP2-deficient mouse models, we now show that LRP2 is expressed in the cardiac progenitor niche of the anterior second heart field (SHF) that contributes to the elongation of the OFT during separation into aorta and pulmonary trunk. Loss of LRP2 in mutant mice results in the depletion of a pool of sonic hedgehog-dependent progenitor cells in the anterior SHF due to premature differentiation into cardiomyocytes as they migrate into the OFT myocardium. Depletion of this cardiac progenitor cell pool results in aberrant shortening of the OFT, the likely cause of CAT formation in affected mice. Our findings identified the molecular mechanism whereby LRP2 controls the maintenance of progenitor cell fate in the anterior SHF essential for OFT separation, and why receptor dysfunction is a novel cause of conotruncal malformation.
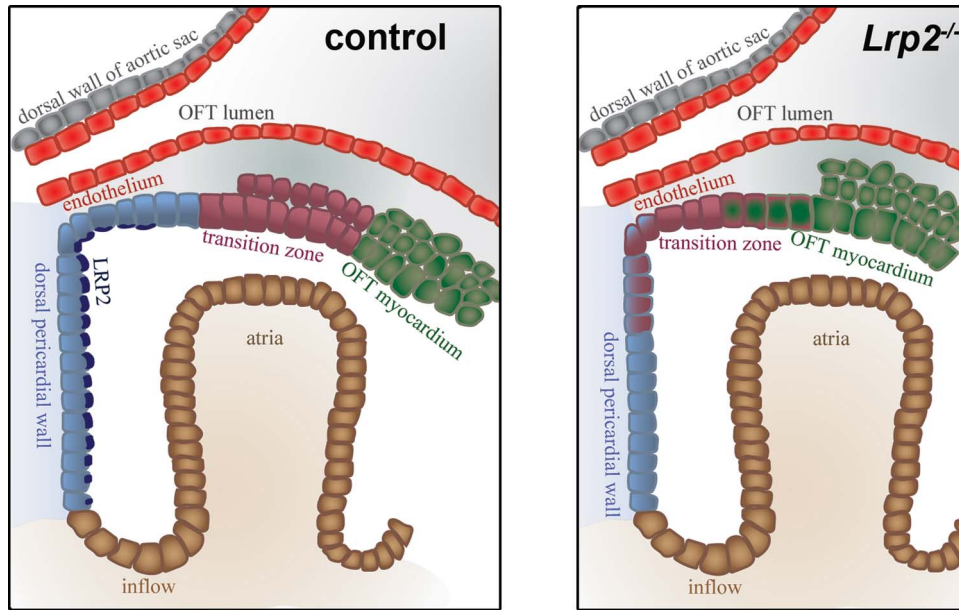
[†]Annabel Christ, http://orcid.org/0000-0002-2019-176X

Graphical Abstract

Introduction

LRP2 is a member of the LDL receptor gene family, a class of multifunctional endocytic receptors that play key roles in embryonic development and that result in severe developmental malformations in humans and animal models when dysfunctional (1). During neurulation, LRP2 is prominently expressed in the neuroepithelium that gives rise to the various parts of the developing central nervous system. Loss of receptor expression in this tissue in gene-targeted mice results in the fusion of the forebrain hemispheres (holoprosencephaly) (2,3) and in the overgrowth of the eye globe (buphthalmia) (4,5). Similar defects are seen in patients with Donnai-Barrow/Facio-oculo-acoustico-renal (DB/FOAR) syndrome, an autosomal recessive disorder caused by inheritable *LRP2* mutations (6–9).

Concerning its mode of action, LRP2 has been shown to act as an auxiliary receptor for sonic hedgehog (SHH) and to activate or inhibit this morphogen pathway dependent on the cellular context. In the neuroepithelium, LRP2 acts as a co-receptor to Patched1 to promote SHH signaling and to pattern the ventral midline of the forebrain (10). In contrast, in the developing eye, it operates as a clearance receptor for SHH to antagonize growth promoting signals by this morphogen in the retina (11). Conceptually, these functions of LRP2 in control of SHH signaling explain the forebrain and eye phenotypes observed in patients with DB/FOAR syndrome. However, LRP2 has also been shown to bind fibroblast growth factor (FGF) 8 (12) and bone morphogenetic protein (BMP) 4 (3) and may thus have the potential to regulate multiple morphogen pathways during organogenesis.

Surprisingly, unbiased screens using exome sequencing now implicated mutations in *LRP2* in congenital heart disease in humans, a receptor function not considered thus far (13). Additional evidence for a role in heart development came with ENU-induced mutagenesis studies that revealed *Lrp2* mutations as a prominent cause of cardiac outflow tract (OFT) defects in mice (14). The cardiac OFT is a transient structure at the arterial pole of the embryonic heart. During development, it separates into the ascending aorta and pulmonary trunk, outlets of the definitive left and right ventricles, respectively. Defects in OFT formation produce conotruncal malformations characterized by incomplete or absent separation of the aorta and pulmonary trunk, resulting in low oxygen supply due to the provision of mixed blood to the circulation. OFT malformations account for almost 30% of all congenital heart defects in humans (15). Recently, a range of cardiac anomalies including CAT but also ventricular septal defects and atrioventricular canal malformations were reported in mice with targeted *Lrp2* gene disruption (16). Still, the molecular mechanism of receptor action in heart development remained unexplained.

In this study, we focused on CAT formation, the most consistent feature of heart malformations observed in *Lrp2* mutant mice. We demonstrate that LRP2 is specifically expressed in SHH-responsive progenitor cells in the dorsal pericardial wall (DPW) that contribute to the formation of the OFT. Loss of receptor activity in *Lrp2* mutant mice impairs SHH signaling in the DPW, resulting in decreased numbers and disturbed myocardial differentiation of progenitors that migrate into the OFT myocardium. Ultimately, these morphogenetic defects cause insufficient elongation of the OFT, which may cause the conotruncal malformations seen in mice, and possible in patients lacking LRP2.

Results

Loss of LRP2 results in formation of a common arterial trunk including defective endocardial cushion formation

To elucidate the molecular mechanism(s) of LRP2 action in mammalian heart development, we studied mice homozygous for a targeted *Lrp2* gene disruption (*Lrp2*$^{-/-}$) generated by us previously (2) and compared them to somite-matched control embryos. *Lrp2* mutant embryos were compared with their respective wild-type or heterozygous littermates, as no defects were observed in *Lrp2*$^{+/-}$ animals. The latter two genotypes are jointly referred to as controls herein.
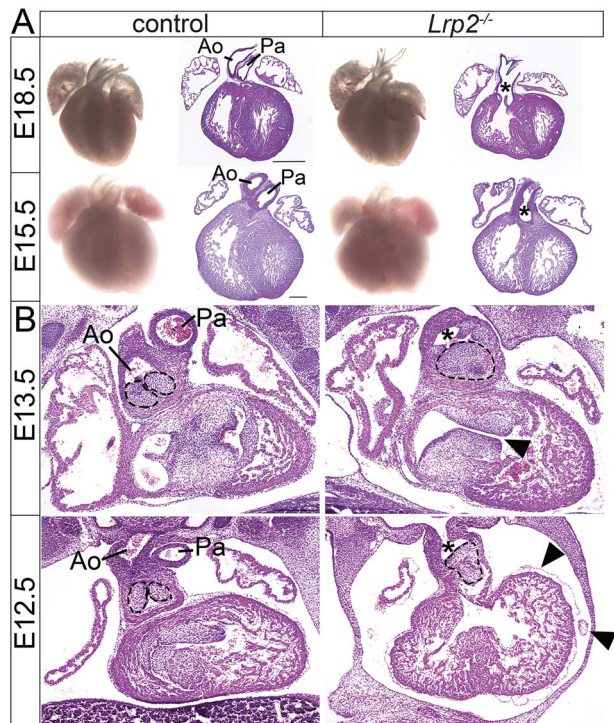
Figure 1. Loss of LRP2 causes the formation of a common arterial trunk. (**A**) Whole mounts (left) and coronal sections (right) of $Lrp2^{-/-}$ and control mouse hearts at embryonic (E) day 18.5 and 15.5. In control embryos, separation of the OFT into aorta (Ao) and pulmonary trunk (Pa) is evident in both embryonic stages. In $Lrp2^{-/-}$ embryos, aorta and pulmonary trunk fail to separate resulting in a common arterial trunk (CAT, indicated by asterisks). This CAT phenotype showed full penetrance and was seen in 23 out of 23 $Lrp2^{-/-}$ embryos analyzed. (**B**) Coronal sections of control and $Lrp2^{-/-}$ hearts at E13.5 and E12.5. In control embryos, aorta (Ao) and pulmonary trunk (Pa) are present. Stippled circles indicate two distinct swellings forming the endocardial cushions in the aortic valve in control hearts. In $Lrp2^{-/-}$ hearts, a common outflow vessel (indicated by asterisks) above the right ventricle is formed. Instead of two endocardial swellings, only one cell cluster in endocardial cushion formation (stippled circle) is apparent. At E13.5, $Lrp2^{-/-}$ embryos display ventricular septal defects (arrowhead). At E12.5, arrowheads indicate blebbing of the epicardium and hemorrhages in $Lrp2^{-/-}$ embryos. Scale bars: A, 750 µm; B, 250 µm.

Loss of LRP2 activity in $Lrp2^{-/-}$ mice leads to defects in OFT formation characterized by incomplete or absent separation of the aorta (Ao) and pulmonary trunk (Pa), a defect referred to as a common arterial trunk (CAT; persistent truncus arteriosus). CAT formation was evident at embryonic (E) day 18.5 and 15.5 when control embryos showed properly separated Ao and Pa (Fig. 1A), while $Lrp2^{-/-}$ embryos exhibited a single vessel exiting the heart from the right ventricle (Fig. 1A, asterisks). Histological alterations indicative of an OFT defect manifested around E12.5 to E13.5 when OFT septation normally occurs. At this time point, septation of Ao and Pa through the formation of the major septal cushions was seen in control but not in LRP2-deficient embryos (Figs 1B and Supplementary Material, S1A). In addition to CAT, other malformations of the heart were also detected in mutant mice, albeit at more variable levels. Thus, some $Lrp2^{-/-}$ embryos failed to form distinct endocardial valve cushions but exhibited only one cell cluster in the common outlet valve (Fig. 1B, stippled circle), the likely cause for the hypoplastic semilunar valves of the common trunk seen in E15.5 mutants (Supplementary Material, Fig. S1B, arrows). Deeper intertrabecular spaces (Supplementary Material, Fig. S1A, arrows), defective formation of ventricular septum (Fig. 1B, arrowhead; Supplementary Material, Fig. S1A,
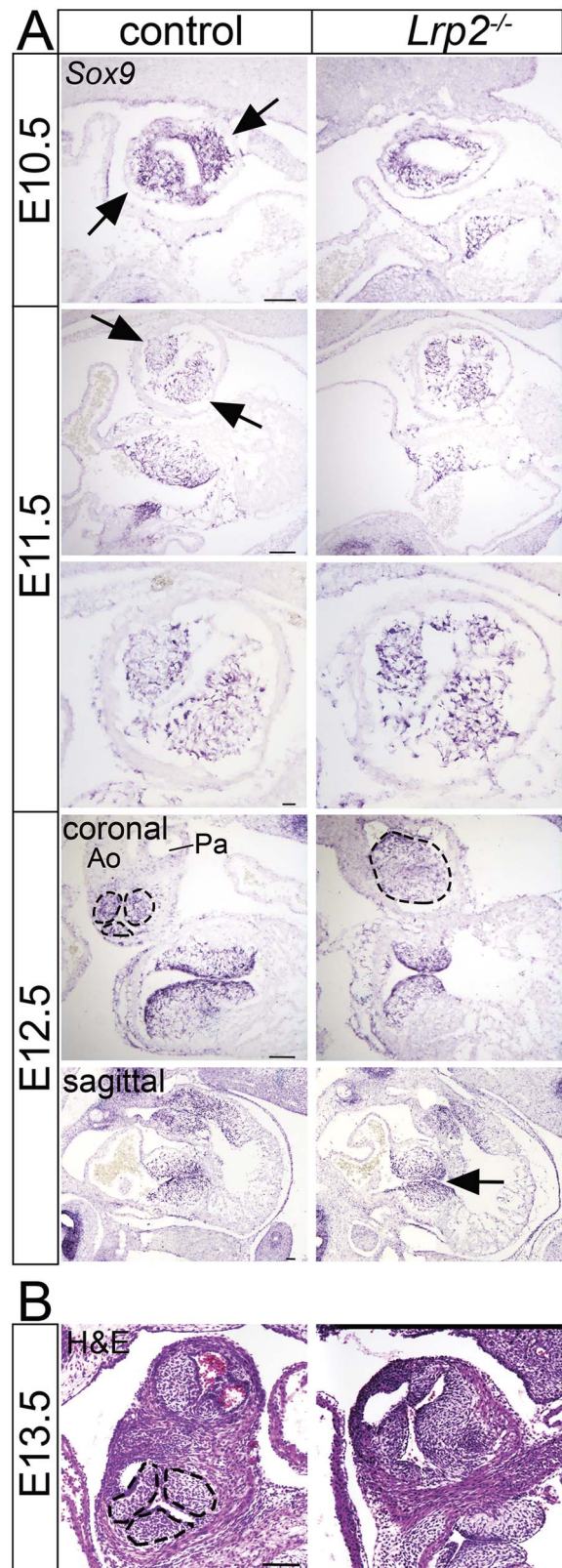
Figure 2. Altered endocardial cushion formation in $Lrp2^{-/-}$ hearts. (**A**) ISH for *Sox9* on coronal and sagittal sections of $Lrp2^{-/-}$ and control embryos depicts endocardial cushion formation in the OFT. At E10.5, two endocardial cushions are formed by two distinct tissue swellings in the control OFT tissue (arrows). In $Lrp2^{-/-}$ OFT tissue, these two tissue swellings are not visible. At E11.5, *Sox9* positive cells cluster in the endocardial cushions (arrows) in control OFT tissue.

arrowhead in E13.5) as well as blebbing of the epicardial cell layer and hemorrhages (Fig. 1B, arrowheads; Supplementary Material, Fig. S1A, arrowheads in E12.5) were other variable pathological features of mutant hearts.

Because the formation of a CAT was the most prominent and most consistent phenotype seen in *Lrp2* mutant mice (100% penetrance), we focused on elucidating its molecular cause in our mouse model of (DB/FOAR) syndrome. Given the importance of the major endocardial septal cushion formation for OFT septation, we compared this process in wild-type and *Lrp2*$^{-/-}$ embryos using *in situ* hybridization (ISH) for *Sox9* (Fig. 2A). *Sox9* is expressed in the cardiac cushion mesenchyme and promotes cardiac valve progenitor proliferation (17). At E10.5, two *Sox9* positive major septal endocardial cushions were visible in control embryos (arrows) while these distinct tissue swellings were not detectable in *Lrp2*$^{-/-}$ embryos, despite the presence of *Sox9* positive cells. By E11.5, these spiraling clusters of *Sox9* positive cells were less compacted in *Lrp2*$^{-/-}$ as compared with control embryos (Fig. 2A, E11.5 lower panel). Of note, ISH for *Sox9* also identified defects in endocardial swellings of the aortic valve that formed an unorganized *Sox9* positive cell cluster in the mutant embryo (Fig. 2, stippled circle in E12.5 *Lrp2*$^{-/-}$ embryo). This defect likely causes the hypoplastic semilunar valves seen in the common trunk in mutants (Supplementary Material, Fig. S1B). In some *Lrp2*$^{-/-}$ embryos, signs of mild hypoplasia of the atrioventricular cushions were observed (Fig. 2A, arrow in E12.5 sagittal). Investigating the formation of aortic valve leaflets at E13.5 in more detail, we observed clearly defined left coronary, right coronary and noncoronary leaflets in the control embryos (Fig. 2B, stippled circles). In contrast, *Lrp2*$^{-/-}$ embryos displayed deformed common valve leaflets at this embryonic stage (Fig. 2B), defects in line with the observation of malformed endocardial cushions at E11.5 (Fig. 2A).

LRP2 is expressed in the progenitor domain of the second heart field

The formation, elongation and septation of the cardiac OFT depends on the interaction of two distinct cell populations, namely cardiac neural crest cells (CNCCs) and second heart field (SHF) cells. CNCCs are a subpopulation of neural crest cells that originate from the dorsal neural tube and that migrate into pharyngeal arches 3, 4 and 6. Starting from E9.5, CNCCs populate the cardiac OFT and move into the OFT cushions (18). There, they give rise to the condensed mesenchyme in the major endocardial septal cushions forming the aorticopulmonary septation complex that divides the distal OFT into Ao and Pa (19). In contrast, SHF cells are cardiac progenitor cells located in the pharyngeal mesoderm. During heart development, they are added to the arterial pole of the OFT driving OFT elongation.

To interrogate the role of LRP2 during OFT formation, we investigated the expression pattern of the receptor during OFT septation using immunohistology. At E9.5 and E10.5, when CNCCs invaded the OFT cushions, LRP2 showed strong expression in the surface ectoderm as well as in the epithelium of the pericardial cavity, including the DPW harboring SHF progenitors. In addition, LRP2 was detected in the epithelium

enveloping the distal OFT (Fig. 3A, E9.5 and E10.5). Upon closer inspection of the distal OFT, LRP2 expression regionalized mainly to the superior and inferior OFT regions (Fig. 3B, coronal view).

From the DPW, progenitor cells move along a path of differentiation via an intermediate state in the transition zone (Tz) to being fully differentiated cardiomyocytes when reaching the OFT myocard (20). To better visualize LRP2 expression along this migratory path, we used higher magnification of a sagittal view of E10.5 control hearts (Fig. 3B, sagittal). In this plane of section, LRP2 levels were high in cells of the DPW but reduced in the Tz and completely absent from the OFT myocardium. This observation argued for a function of LRP2 in SHF progenitors that was lost as differentiation to cardiomyocytes proceeded. At E12.5, when the OFT was already septated, robust LRP2 expression persisted in the DPW and in the epithelial sheet enclosing the most distal regions of the Ao and Pa, while only minor receptor levels were visible in tissue surrounding the atria and ventricles (Fig. 3A, arrowheads in E12.5). LRP2 was absent from cardiomyocytes and endothelial cells as documented by lack of co-expression with cardiomyocyte marker alpha-smooth muscle actin (SMA) and endothelial cell marker platelet endothelial cell adhesion molecule (PECAM) (Fig. 3A, lower panel in E12.5).

LRP2 deficiency specifically impacts SHF progenitor cells

While LRP2 expression in neural crest cells had been reported before (19,20), we failed to detect the receptor in the CNCC population using immunohistology (Fig. 4A). Still, the major septal cushion defect observed in *Lrp2*$^{-/-}$ embryos was consistent with a potential defect in CNCCs. To query an indirect effect of receptor deficiency on this cell population, we crossed the *Lrp2* deficient mouse strain with the *Wnt1-Cre_LacZ* reporter line to specifically mark CNCCs (23). Staining lacZ activity at E10.5 revealed a comparable pattern of CNCCs in the OFT of *Lrp2*$^{-/-}$ and control embryos (Fig. 4B). Subtle differences were seen in more proximal regions of the spiraling OFT cushions, where CNCCs appeared less compacted in *Lrp2*$^{-/-}$ embryos compared with controls (Fig. 4B, stippled circle). Based on these data, we concluded that LRP2 deficiency did not profoundly impact the migration of CNCCs into the OFT or their integration in the major septal cushions. Rather subtle alterations in CNCC organization seen in the proximal OFT of mutant mice were considered secondary to defects in cushion formation.

Since *Lrp2* deficiency did not affect the migration of CNCC, we turned our attention to SHF cells that express LRP2 and that are necessary for OFT septation. Among other markers, these cells are characterized by the expression of insulin gene enhancer protein (*Islet1*) (24). Islet1 protein as well as *Islet1* transcript showed decreased expression levels in the pharyngeal mesoderm and in the OFT of *Lrp2*$^{-/-}$ embryos compared with controls (Fig. 5A and B) possibly explaining defective OFT development. Islet1 protein and transcript were especially reduced in the superior and inferior intercalated cushions, which were visible at E11.5 in both genotypes (Fig. 5A and B, arrowheads). Reduced levels of Islet1 in the intercalated cushions likely contribute to

In mutants, *Sox9* positive cells are less compacted and poorly organized in the endocardial cushions as depicted in the higher magnification view at E11.5. At E12.5 in control OFT tissue, the OFT septum has formed and divides aorta (Ao) and pulmonary trunk (Pa). *Sox9* positive cells are localized in the endocardial swellings of the aortic valve (stippled circles), while in *Lrp2*$^{-/-}$ OFT vessel, only a disorganized cluster of *Sox9* positive cells is visible (stippled circle). On E12.5 sagittal sections (arrow), mild hypoplasia of the atrioventricular cushions with a loss of fusion is observable in *Lrp2*$^{-/-}$ embryos compared with controls. (**B**) Hematoxylin and eosin-stained coronal sections of *Lrp2*$^{-/-}$ and control embryos at E13.5 documenting the left coronary, right coronary and noncoronary leaflets in the aortic valve of control embryos (stippled circles) but malformed common valve leaflets in *Lrp2*$^{-/-}$ embryos. Scale bar: 100 μm.
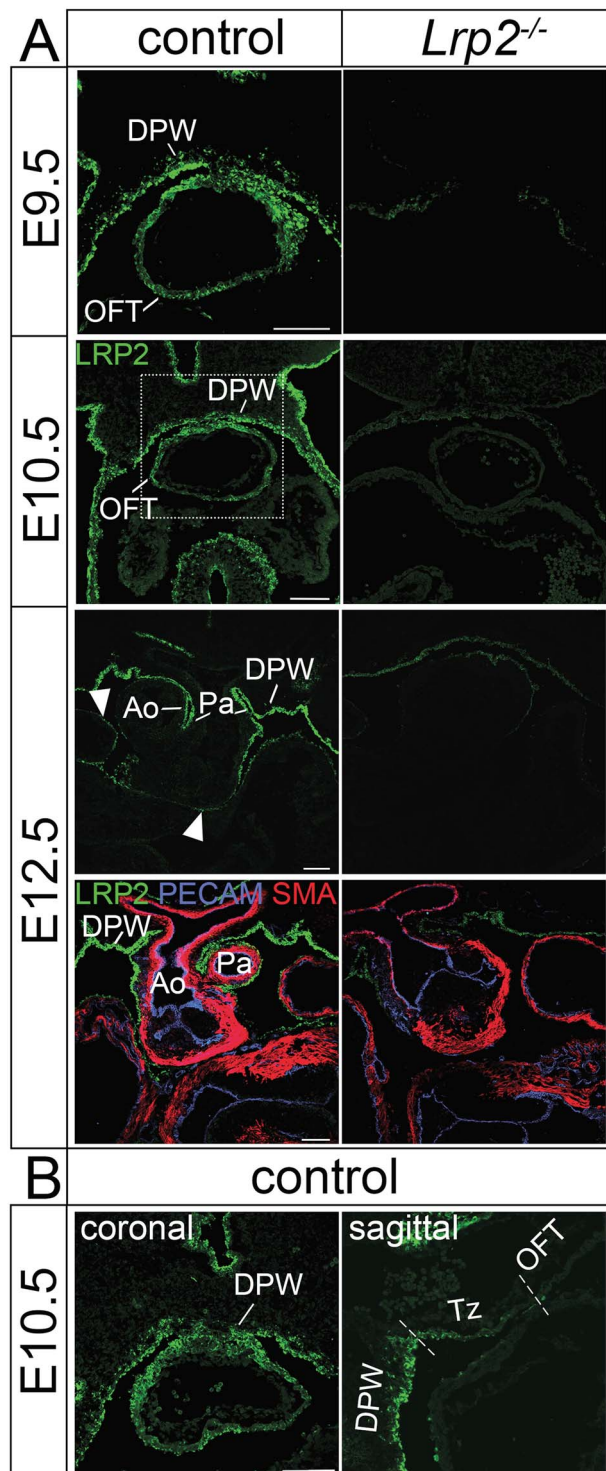
Figure 3. LRP2 expression in the developing OFT. Immunhistological detection of LRP2, SMA, and PECAM on the coronal sections of the embryonic mouse heart at the indicated embryonic days. (**A**) At E9.5 and E10.5, LRP2 expression is seen along the ectoderm as well as in the epithelium enclosing the pericardial cavity, including the DPW and in the distal OFT myocardium of controls. No immunoreactivity for LRP2 is detected in receptor mutant hearts. At E12.5, LRP2 expression is visible in the DPW and in myocardial cells surrounding the pulmonary artery (Pa) as well as the aorta (Ao) at the side facing the Pa. Minor LRP2 levels are visible in the epithelium enveloping atria and ventricles (arrowheads). Cardiomyocytes are stained with SMA and endocardial cells are stained with PECAM. (**B**) Higher magnification of the region corresponding to the boxed area in control embryos in panel

the defective development of the common non-coronary valve leaflet observed in *Lrp2*$^{-/-}$ hearts (Fig. 2B).

To investigate which cells in the SHF express LRP2, we studied its localization with respect to SHF marker Islet1 and cardiac mesoderm marker NK2 transcription factor-related locus 5 (Nkx2–5), a myocardial transcription factor regulated by Islet1 and required for SHF development. LRP2 was expressed in the DPW (Fig. 5C, arrow) but also in the epithelial sheet surrounding the intercalated cushions in the OFT (Fig. 5C, arrowheads), partially overlapping in these regions with Nkx2–5 and Islet1 in controls. In *Lrp2*$^{-/-}$ mutants, Nkx2–5 protein in the distal OFT was less restricted to the superior and inferior regions (Fig. 5C, stippled lines in control embryos) but showed a more widespread localization throughout the distal OFT. Islet1 demonstrated decreased levels in the pharyngeal mesoderm (Fig. 5A and C, asterisks) as well as in the superior and inferior intercalated cushions (Fig. 5A arrowheads; Fig. 5C arrows).

We also tested the expression of two additional SHF markers, namely neurovascular guiding factor *Sema3c*, important to correctly navigate CNCCs towards the OFT (25), as well as *T-box transcription factor 1* (*Tbx1*), stimulating the proliferation of multipotent heart progenitors (26). Overall, the expression pattern of *Sema3c* was largely unchanged in *Lrp2*$^{-/-}$ embryos compared with controls, although slightly reduced levels were noted in the intercalated cushions of the OFT (Supplementary Material, Fig. S2A, arrowheads). Also, expression levels of *Tbx1* were comparable between genotypes (Supplementary Material, Fig. S2B), suggesting mis-patterning rather than complete absence of SHF progenitors in LRP2 mutant mice.

LRP2 promotes SHH signaling during OFT formation

So far, our data documented a decrease in Islet1-positive SHF progenitor cells and a shifted localization of Nkx2–5 positive cells in LRP2 mutant embryos, arguing for a role of this receptor in controlling cardiac progenitor maintenance during OFT septation. Several signaling pathways have been implicated in the formation, proliferation and differentiation of multipotent cardiac progenitor cells in the SHF, including signaling through Wnts, BMPs and SHH (27). Since LRP2 is known to act in multiple morphogen pathways, we investigated these pathways in *Lrp2*$^{-/-}$ embryos during OFT development.

Canonical Wnt signaling has been shown to act upstream of other signaling pathways in control of Islet1-positive progenitor cell proliferation (28). Non-canonical Wnt signaling is implicated in OFT development (26,27) and important for planar cell polarity during myocardialization of the OFT cushions. It regulates polarity and intracellular cytoskeletal rearrangements, important to prevent premature differentiation of SHF progenitor cells into cardiomyocytes (31–33). To explore potential defects in canonical Wnt signaling during OFT formation, we crossed the *Lrp2* mutant strain with the *Tcf/Lef_LacZ* reporter line. Detecting lacZ activity as a read-out of Wnt signaling, we failed to observe any changes in Wnt activity in the SHF of embryos lacking LRP2 (Supplementary Material, Fig. S3A). Also, the non-canonical Wnt pathway was unchanged as deduced from investigating the expression pattern of *Wnt11* in the OFT using ISH (Supplementary Material, Fig. S3B). BMP signaling downregulates proliferation when SHF cells enter the OFT and drives myocardial differentiation (34). Analyzing the BMP pathway by studying *Bmp4* expression in the distal OFT, we failed to detect obvious changes in LRP2-deficient as compared with control embryos (Supplementary Material, Fig. S3B).
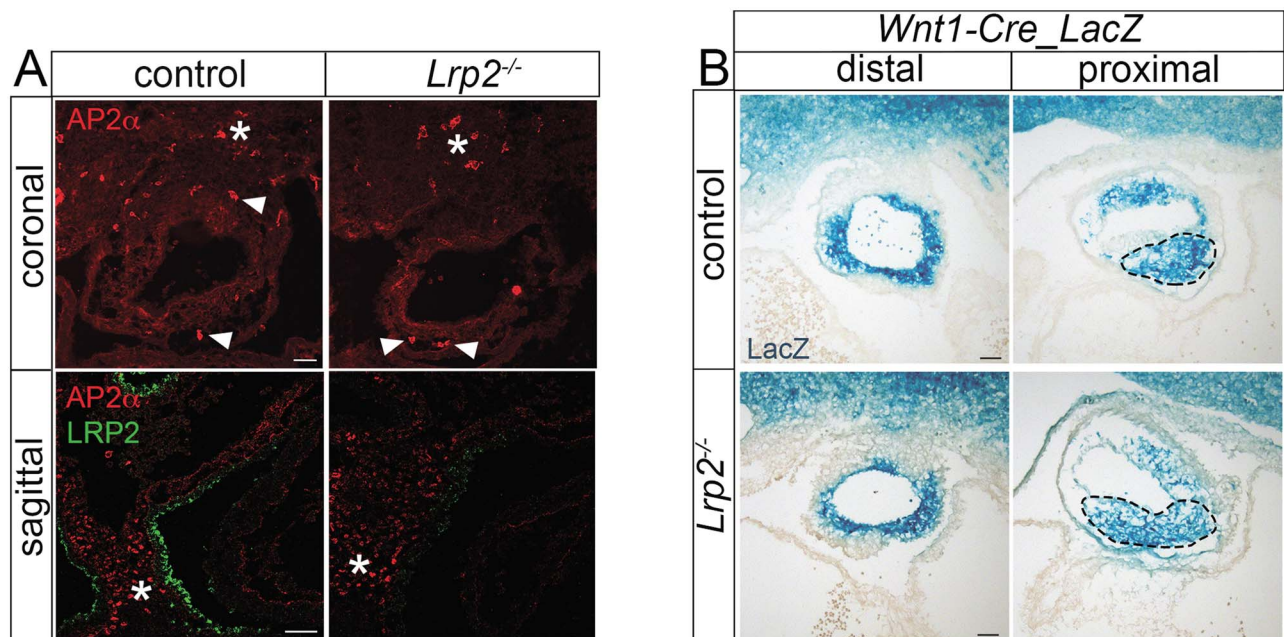
Figure 4. LRP2 deficiency does not affect the CNCC population migrating into the OFT. (**A**) Immunohistological detection of AP2α on coronal and of AP2α and LRP2 on sagittal sections of the hearts of control and $Lrp2^{-/-}$ embryos at E10.5. Similar numbers of AP2α positive cells are detected in the SHF region (asterisks) and in the OFT (arrowheads) of $Lrp2^{-/-}$ and control embryos. AP2α and LRP2 show non-overlapping expression domains, suggesting the absence of LRP2 from CNCCs. (**B**) Staining for lacZ activity in CNCCs on coronal sections of E10.5 mouse OFT tissues from the *Wnt1-Cre_LacZ* reporter line. Mice express (control) or lack LRP2 ($Lrp2^{-/-}$). In sections of the distal OFT region (left panels), the presence of CNCCs in the outflow vessel is detected in control and $Lrp2^{-/-}$ embryos. In more proximal regions of the OFT (right panel), CNCCs fail to accumulate in the endocardial cushions in $Lrp2^{-/-}$ as compared with the control OFT vessel (stippled circle). Scale bars: 50 μm.

Another essential morphogenetic signal in SHF patterning is provided by SHH secreted from the pharyngeal endoderm. SHH regulates both CNCC survival and OFT development (35). Using the *Gli1-LacZ* reporter allele introduced into the *Lrp2* mutant strain, we detected reduced SHH activity in the distal OFT of $Lrp2^{-/-}$ embryos as compared with controls (Fig. 6). At 28 somites even before intercalated cushion, developed SHH activity is already reduced. Still, we cannot exclude that impaired formation of the intercalated cushions may also secondarily contribute to the reduction in Gli1_lacZ activity seen in the mutant tissue. Nevertheless at 30 and 32 somites, reduced SHH activity was especially evident in the inferior OFT region where SHH signaling was significantly decreased in LRP2-deficient embryos (Fig. 6). To test if reduced SHH signaling in $Lrp2^{-/-}$ embryos was connected to the SHF defects as characterized by reduced *Islet1* expression, we crossed the LRP2-deficient line with the *Gli1-CreER*[T2] reporter strain. In this line, expression of a tamoxifen-inducible Cre transgene under control of the *Gli1* promoter enables labeling of SHH-responsive cells by Cre-induced expression of YFP (36). To induce YFP expression, pregnant mice were injected with tamoxifen at E7.5 and embryos were analyzed at E10.5. Immunodetection of YFP demonstrated SHH-responsive cells accumulating in the inferior OFT region in control embryos (Fig. 7A). In $Lrp2^{-/-}$ embryos, YFP-positive cells were reduced about 50% in numbers and failed to accumulate in the inferior OFT region (Fig. 7A, arrowheads; Fig. 7B).

Next, we performed co-immunostaining for YFP and Islet1 to test if SHF progenitor cells lacking LRP2 were less responsive to SHH signals. YFP positive cells in the inferior OFT of control embryos co-immunostained with Islet1. $Lrp2^{-/-}$ embryos showed a significant reduction in Islet1 immunoreactivity in the pharyngeal mesoderm (Fig. 7A, asterisk) as well as in the superior and inferior OFT (Fig. 7A, arrowheads). Quantification of cardiac progenitor cells double positive for Islet1 and YFP substantiated a significant reduction of SHH-responsive Islet1-positive progenitor cells in the distal OFT of LRP2-deficient embryos (Fig. 7C).

During OFT formation, SHF progenitor cells located in the DPW move along a path of differentiation to the Tz, where they initiate a myocardial gene expression program. They finally reach the OFT myocardium to fully differentiate into cardiomyocytes. By this movement, cardiac SHF progenitor cells contribute to the elongation of the OFT, necessary for correct alignment. Disturbances in this differentiation program result in a shortened OFT and can give rise to a CAT (37). A significant decrease in OFT length was seen in the hearts of $Lrp2^{-/-}$ embryos compared with controls (Fig. 7D and E), arguing for a defect in progenitor movement in $Lrp2^{-/-}$ embryos.

To investigate the consequences of reduced SHH signaling in DPW progenitors for their differentiation potential, we studied sagittal sections of *Gli1-CreER*[T2] control and LRP2-deficient embryos at E10.5. In controls, SHH-responsive cells (as deduced by YFP expression) concentrated in the DPW and distal Tz, a

A. On a coronal view (left panel), robust LRP2 expression is seen in cells of the SHF in the DPW and in distal myocardial cells of the OFT. In the OFT, LRP2 immunoreactivity is most prominent in the superior and inferior OFT regions. On a sagittal view (right panel), prominent levels of LRP2 are seen in epithelial cells of the DPW. Receptor expression is significantly reduced in the Tz and completely absent from the proximal OFT myocardium (OFT). Boundaries between DPW, TZ and OFT myocardium are marked by stippled white lines. Scale bar: 100 μm.
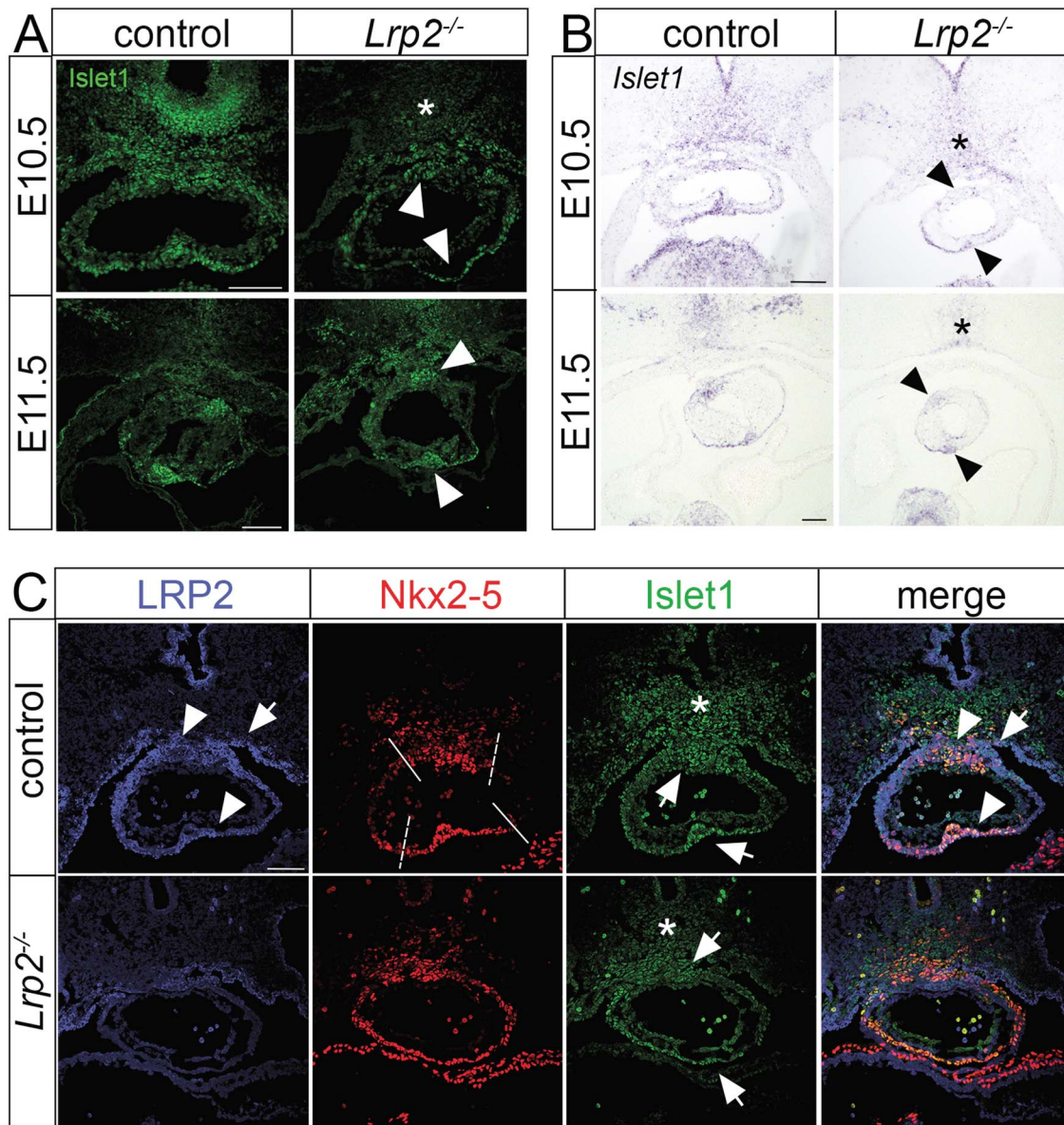
Figure 5. a reduction in SHF cardiac progenitor cells. (**A**) Immunodetection of Islet1 and (**B**) ISH for *Islet1* on coronal OFT sections of control and *Lrp2*$^{-/-}$ embryos at E10.5 and E11.5. In *Lrp2*$^{-/-}$ embryos, immunosignals for Islet1 are decreased in the pharyngeal mesoderm (A, asterisk) and in the superior and inferior intercalated cushions of the OFT (A, arrowheads) when compared with controls. The reduction in Islet1 protein levels in mutants is paralleled by decreased *Islet1* transcript levels at both embryonic stages in the pharyngeal mesoderm (B, asterisk) and in the intercalated cushions (B, arrowheads) as compared with controls. Scale bar: 100 μm. (**C**) Immunohistological detection of LRP2, of SHF marker Nkx2–5 and of SHF cardiac progenitor marker Islet1 on coronal sections of E10.5 control and *Lrp2*$^{-/-}$ embryos. Single channels as well as merged images are shown. Cardiac progenitor cells of the SHF in the DPW (arrow in LRP2 and merged channels) and in the myocardium lining the intercalated cushions (arrowheads in LRP2 and merged channels) stain positive for LRP2. Lack of LRP2 in *Lrp2*$^{-/-}$ embryos results in the presence of Nkx2–5 positive cells throughout the OFT. This contrasts with the more restricted pattern in the superior and inferior OFT region (stippled white lines) in the control embryo. Furthermore, *Lrp2*$^{-/-}$ embryos show reduced numbers of Islet1 positive cells in the pharyngeal mesoderm (asterisk in single channel) as well as in the intercalated cushions (arrows in single channel) when compared with controls. Scale bar: 75 μm.

region overlapping with the LRP2 expression domain in the DPW (Fig. 8A). Very few SHH-responsive cells were detected in the OFT myocardium of control embryos as evidenced by almost complete absence of co-staining of YFP with the cardiomyocyte marker MF20 (Fig. 8A). In contrast, in *Lrp2*$^{-/-}$ embryos, an increased number of SHH-responsive cells were co-stained by YFP and MF20 in the OFT myocardium (Fig. 8A, arrowheads). Quantification of YFP and MF20 double positive cells corroborated this observation, demonstrating a significant increase in YFP-MF20 double positive cells in the OFT

myocardium in *Lrp2*$^{-/-}$ embryos (Fig. 8B). Jointly, the reduction of YFP/Islet1 double positive cells in the distal OFT and the increased amount of YFP/MF20 double positive cells in the OFT myocardium in *Lrp2*$^{-/-}$ embryos argued for a role of LRP2 in facilitating the response of SHF progenitors in the DPW to SHH. Such a response is required to control migratory movement and differentiation along their path to the OFT myocardium. Reduced responsiveness to SHH in the LRP2-deficient DPW was not due to the impaired formation of primary cilia, essential for SHH signal reception, as documented by staining for the
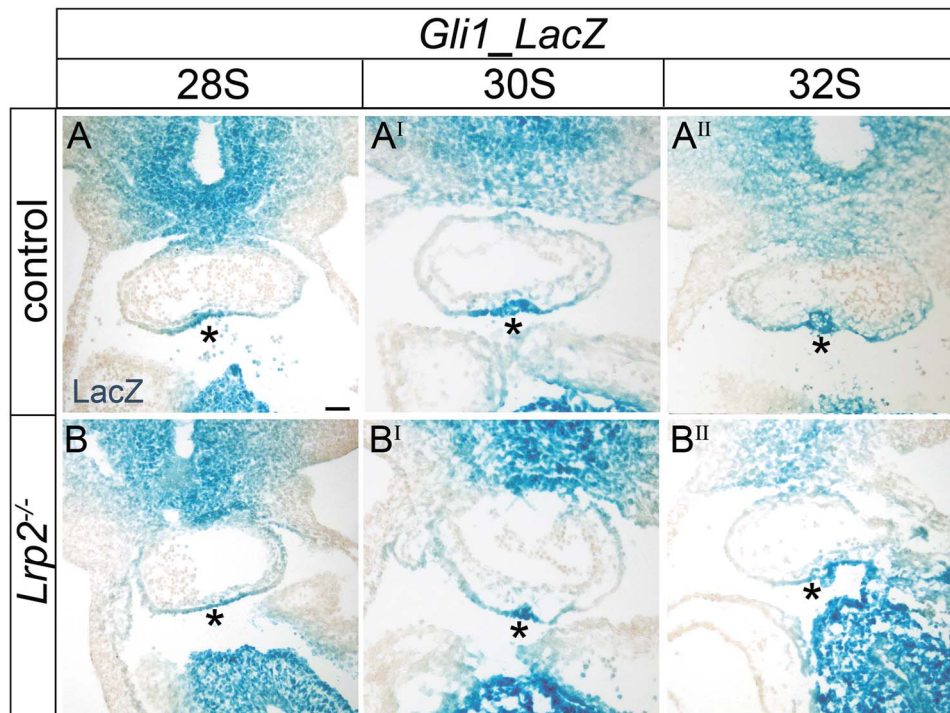
Figure 6. Reduced SHH signaling activity in the *Lrp2*$^{-/-}$ OFT. Staining for lacZ activity on coronal sections from 28 somites, 30 somites and 32 somites old *Gli1_LacZ* reporter embryos to visualize SHH signaling. Animals express (control) or lack LRP2 (*Lrp2*$^{-/-}$). In all three examples, the activity of the GLI1-dependent LacZ reporter is significantly reduced in *Lrp2*$^{-/-}$ embryos compared with their somite-matched control (compare asterisks in B to A, B^{I} to A^{I}, in B^{II} to A^{II}). Scale bar: 50 μm.

ciliary marker Arl13b in Islet1-positive progenitor cells in both genotype groups (Supplementary Material, Fig. S4).

LRP2 defines the boundary of the cardiac SHF progenitor zone

To further substantiate a role for LRP2 in control of SHF progenitor cell differentiation along a path from the DPW to the Tz and finally to the OFT myocardium, we performed immunodetection of markers representative of these three tissues in control- and receptor-deficient embryos. Previous studies demonstrated an atypical apicobasal polarization of SHF progenitor cells and their basal filopodia in the DPW, and their increasing epithelial characteristics in the Tz before differentiation in the OFT myocardium (20,26,32,38–40). Therefore, we focused on the immunodetection of proteins having a role in apical cell polarity comparing patterns in DPW and Tz of mutant and control embryos. Immunodetection of the apical tight junction marker aPKC-ζ (41) demonstrated robust expression at the apical cell membrane in the DPW of controls (Fig. 8C). No changes in signal intensity or localization in aPKC-ζ were detected in the *Lrp2*$^{-/-}$ DPW, arguing against an overall effect of LRP2 deficiency on polarization of cells. However, the result was different for the adherens junction marker E-cadherin. Although localization of E-cadherin to the apical cell membrane was comparable between the two genotypes, the distribution of E-cadherin-positive cells was clearly shifted in the mutants. As shown in Fig. 8C, in controls, E-cadherin was expressed in the anterior DPW and further increased in expression in the Tz, consistent with an increasing epithelial cohesion before cells differentiate into OFT myocardium. Vanishing E-cadherin protein levels were detected in the posterior region of the DPW closer to the venous pole. In contrast, in *Lrp2*$^{-/-}$ embryos, the localization of E-cadherin-positive cells in the DPW was shifted to more

posterior regions in the DPW (Fig. 8C, compare localization of the stippled lines). This shifted cell identity was also confirmed by a shift in localization of cardiac troponin I, a marker for mature cardiomyocytes (Fig. 8C). Cardiac troponin I was exclusively expressed in cells of the OFT myocardium in controls. In *Lrp2*$^{-/-}$ OFT tissue, also cells in the TZ stained positive for this protein. Furthermore, laminin, a marker for the basal lamina, also showed an altered localization in *Lrp2*$^{-/-}$ embryos. While in the control DPW and Tz, laminin showed a punctuated pattern in apical cell regions; this punctuated pattern was lost in the *Lrp2*$^{-/-}$ DPW and Tz (Fig. 8C, arrowheads). Finally, in control embryos, the basal lamina formed a continuous pattern in the OFT region but not in the Tz, whereas in *Lrp2*$^{-/-}$ hearts, this continuous pattern of the basal lamina reached inside the Tz (Fig. 8C). Collectively, these findings argued for a reduction in numbers and for premature differentiation of *Lrp2*$^{-/-}$ SHF progenitor cells as they transit from the DWP via the Tz into OFT myocardium. These defects confound the contribution of SHF progenitors to OFT elongation and result in OFT shortening, the likely cause of CAT formation in *Lrp2*$^{-/-}$ mice.

Discussion

Previous studies implicated LRP2 in OFT formation (16). Still, the exact mechanism whereby this multifunctional endocytic receptor may control the formation of the cardiac OFT and why receptor dysfunction results in conotruncal malformations in patients and in mouse models remained unexplained. Here, we uncovered a crucial role for LRP2 in SHH signaling in progenitor cells of the DPW, signals required to ensure their timely differentiation into mature cardiomyocytes as they migrate into the OFT tissue. Loss of LRP2 results in a decrease in SHH-responsive progenitor cells in the DPW and in a concomitant appearance
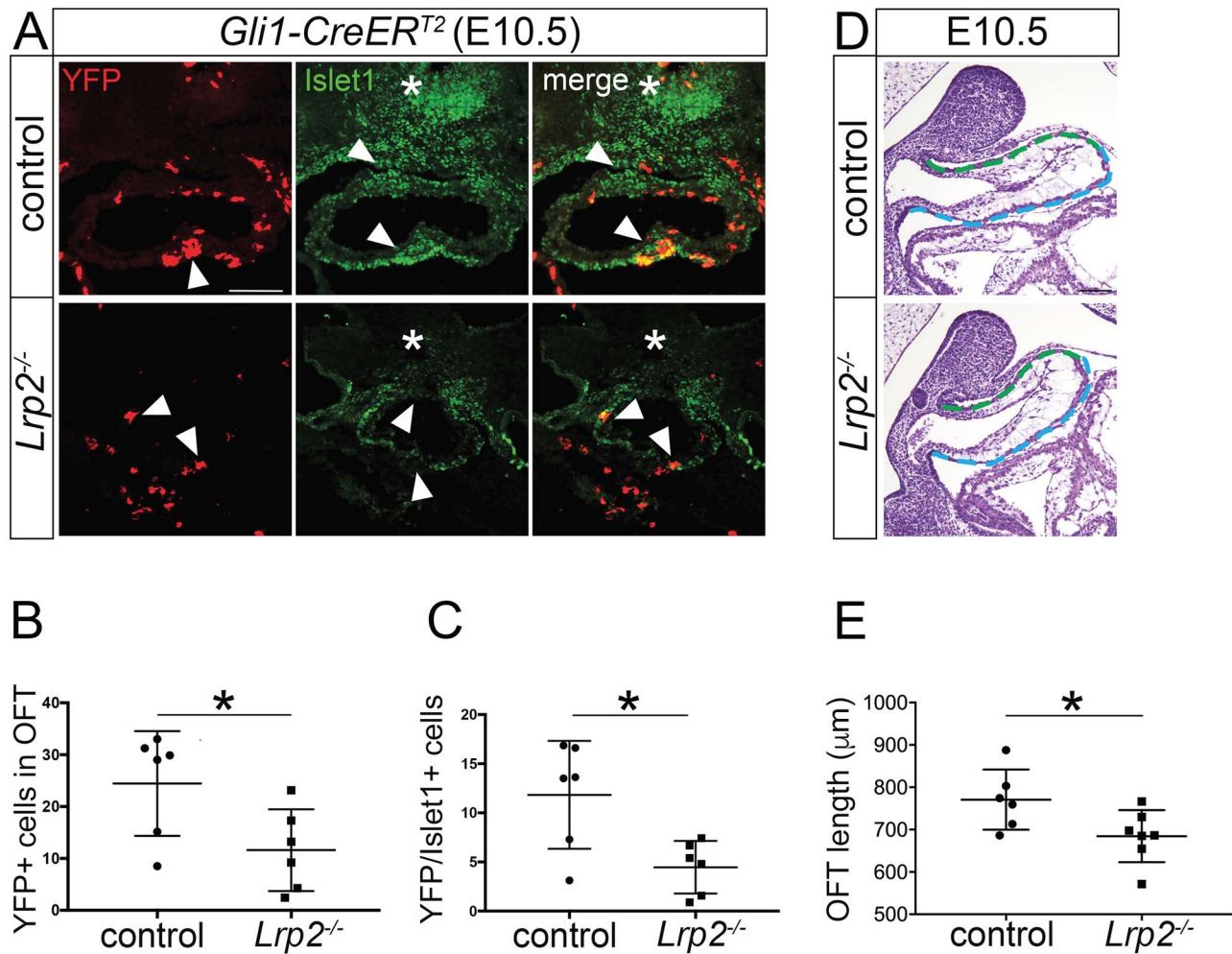
Figure 7. Reduced SHH responsiveness of cardiac progenitor cells in the $Lrp2^{-/-}$ OFT. (**A**) Immunohistological detection of YFP and Islet1 on coronal sections of E10.5 mouse hearts from the tamoxifen-inducible $Gli1$-$CreER^{T2}$ reporter strain. The animals express (control) or lack LRP2 ($Lrp2^{-/-}$). Single channels as well as merged images are shown. In control embryos, YFP-labeled cells are visible throughout the OFT but accumulate in the inferior intercalated cushion (arrowhead). Islet1-positive cardiac progenitor cells are seen in the pharyngeal mesoderm (asterisk) as well as in the superior and inferior OFT (arrowheads). In $Lrp2^{-/-}$ embryos, YFP positive cells fail to accumulate in the inferior OFT but are dispersed throughout the OFT vessel (arrowheads). Also, Islet1 positive cells are reduced in the pharyngeal mesoderm (asterisk) and in the OFT vessel (arrowheads). Scale bar: 100 µm. (**B**) YFP positive cells (as exemplified in panel A) were quantified on 5–9 coronal sections through the distal OFT vessel of 6 control and 6 $Lrp2^{-/-}$ embryos. YFP positive cells are reduced about 50% in $Lrp2^{-/-}$ embryos. (**C**) Cardiac progenitor cells double positive for Islet1 and YFP (as exemplified in panel A) were quantified on 5–9 coronal sections through the distal OFT vessel of 6 control and 6 $Lrp2^{-/-}$ embryos. The numbers of YFP/Islet1 double positive cells in the OFT are significantly reduced in mutant as compared with control embryos (*$P \leq 0.05$; unpaired Student's t test). (**D**) Exemplary hematoxylin and eosin-stained sagittal sections of $Lrp2^{-/-}$ and control embryos at E10.5. The OFT length was determined by taking the average of the measured upper (green line) and lower (blue line) OFT wall lengths for each section. Scale bar: 100 µm. (**E**) OFT length in control and $Lrp2^{-/-}$ OFT tissues as quantified on 5 sagittal sections each through the OFT vessel of 6 control and 7 $Lrp2^{-/-}$ embryos. OFT length is significantly reduced in mutant as compared with control embryos (*$P \leq 0.05$; unpaired Student's t test).

of cardiomyocytes in the Tz, documenting depletion of this progenitor niche due to premature differentiation of cardiac progenitors along their path to an OFT myocardial fate.

Loss of anterior SHF progenitors is the likely cause of CAT formation in $Lrp2^{-/-}$ embryos

Formation and subsequent septation of the OFT is dependent on two cell populations: the SHF and the CNCCs. We traced the primary defect in LRP2 deficiency to the progenitor cells in the anterior SHF that express this receptor (Fig. 5C). While the CNCC population normally migrated into the OFT to reach the distal OFT cushions (Fig. 4), the number of Islet1-positive SHF progenitor cells was significantly reduced in receptor-deficient hearts (Fig. 5). Cardiac progenitors in the DPW contribute to the growth and elongation of the OFT, a process essential for proper septation into Ao and Pa (37). $Lrp2^{-/-}$ mice exhibited

a significantly shortened OFT (Fig. 7E), most likely due to a reduced number of incorporated myocardial cells derived from a diminished progenitor pool in the anterior SHF. In addition to OFT elongation, SHF progenitors also contributed to the formation of the intercalated cushions and, to a minor extent, to the OFT cushion mesenchyme (42). Conceptually, impaired OFT cushion formation in $Lrp2^{-/-}$ mice may be a secondary consequence of OFT shortening in these animals (Fig. 7 D, E). More excitingly, defects in intercalated cushions as well as in the OFT cushions may be explained by a role for LRP2 in also controlling migration of SHF progenitor cells into these tissues. This hypothesis is supported by the malformed formation of OFT cushions (Fig. 2) and by the reduced number of Islet1-positive cells seen in the intercalated cushions of $Lrp2^{-/-}$ mice (Fig. 5) caused by reduced cell migration from the SHF inside these tissues.
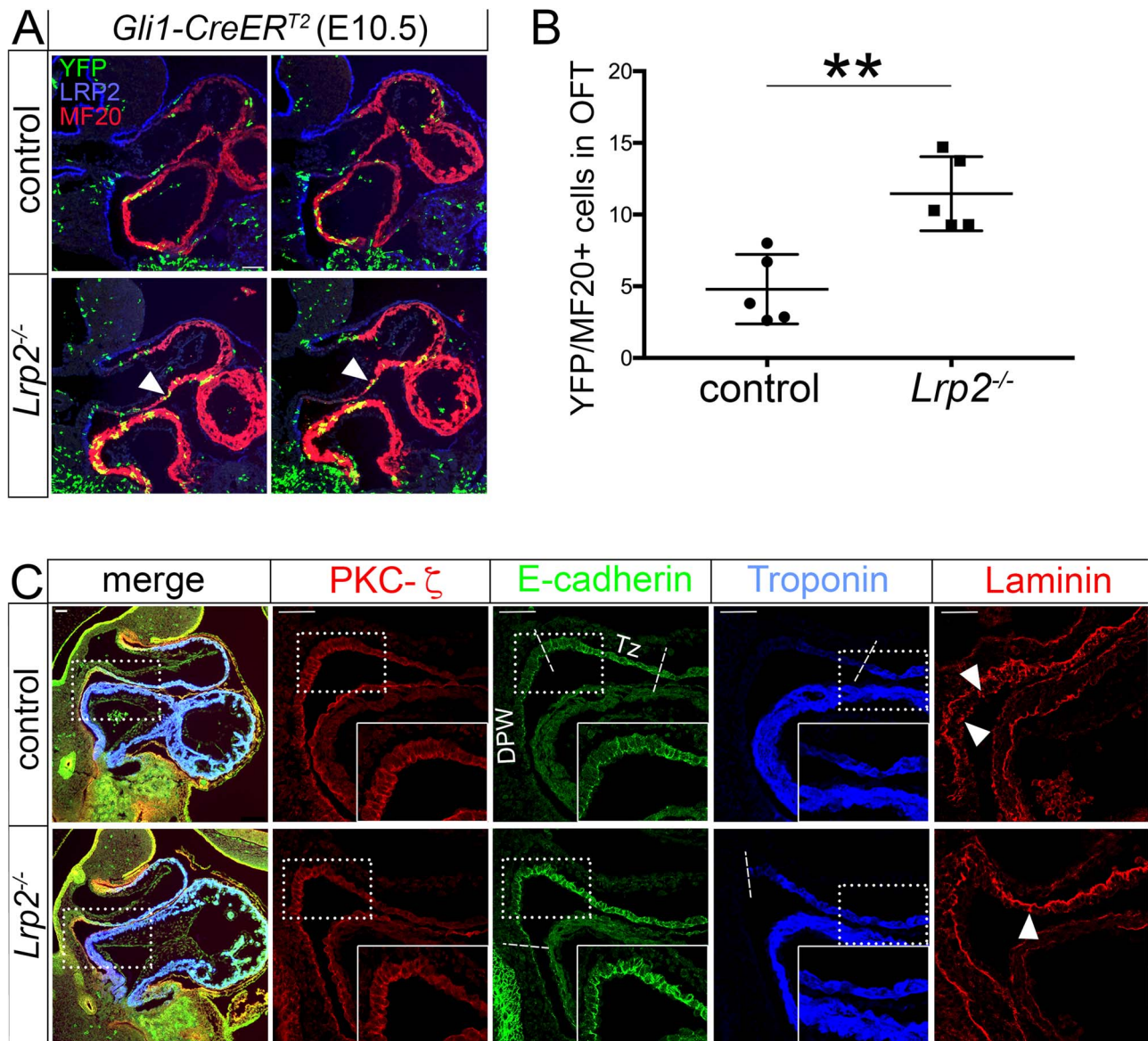
Figure 8. Loss of LRP2 decreases the SHF progenitor niche. (**A**) Immunodetection of YFP (green), LRP2 (blue) and MF20 (red) on two exemplary sagittal sections for E10.5 control and for *Lrp2*$^{-/-}$ hearts of the *Gli1-CreER*^{T2} reporter line. In control embryos, SHH responsive (YFP positive) cells cluster at the border between DPW and Tz (arrow). Very few double positive cells for YFP-MF20 are detected in the OFT myocardium of control embryos. In the two *Lrp2*$^{-/-}$ heart tissue sections, MF20-positive cardiomyocytes in the OFT myocardium are positive for YFP (arrowhead), indicating aberrant differentiation of SHH responsive cells. Scale bar: 100 μm. (**B**) Cardiomyocytes double positive for MF20 and YFP (as exemplified in panel A) were quantified on 5–8 sagittal sections through the OFT vessel of 5 control and 5 *Lrp2*$^{-/-}$ embryos. The numbers of YFP/MF20 double positive cells in the OTF are significantly reduced in mutant as compared with control embryos (**P ≤ 0.01; unpaired Student's *t* test). (**C**) Immunohistological detection of PKC-ζ, E-cadherin, troponin and laminin on sagittal sections of E10.5 control and *Lrp2*$^{-/-}$ heart tissues. To visualize the overall morphology of the heart, merged overview pictures are shown for both genotypes. Detailed comparison of PKC-ζ, E-cadherin, troponin and laminin immunosignals are given in single channel configuration in higher magnification images (boxed areas in overview pictures). The insets depict cellular localization of PKC-ζ, E-cadherin and troponin corresponding to the boxed area in the higher magnification images. Signal intensity and distribution for adherens junction component PKC-ζ (red) are unchanged comparing control and *Lrp2*$^{-/-}$ hearts. In control hearts, E-cadherin (green) exhibits strong expression in the Tz but reduced levels in the DPW. In *Lrp2*$^{-/-}$ hearts, the E-cadherin expression domain extends into the DPW (to the stippled line). Troponin (blue) marks differentiated cardiomyocytes in the OFT myocardium. In contrast to control hearts, troponin expression extends from the OFT myocardium into the transition zone (stippled line) in *Lrp2*$^{-/-}$ hearts. Laminin, a marker for the basal lamina, shows a punctuated pattern with apical vesicles (arrowheads) in the DPW and distal Tz in controls. In *Lrp2*$^{-/-}$ hearts, laminin-positive apical vesicles are reduced in numbers (arrowhead) and the regular pattern of the basal lamina from the OFT continues into the Tz and DPW. Scale bar: 50 μm.

LRP2 deficiency impairs SHH-dependent maintenance of the DPW progenitor zone

To facilitate OFT elongation, SHF progenitor cells exhibit an increased proliferative capacity and a delayed propensity to differentiate into myocardium (43). Several signaling pathways have been implicated in balancing proliferative versus differentiation fate decisions in the SHF (24,39). These pathways include canonical and non-canonical Wnt signaling, as well as signals downstream of FGF, BMP and SHH (27,40–46). Our studies failed to provide evidence for defects in Wnt and BMP signaling as a primary cause of CAT formation in the LRP2-deficient heart (Supplementary Material, Fig. S3). Rather, our findings

from *Gli1_LacZ* (Fig. 6) and *Gli1_CreER*^T2 (Figs 7A–C and 8A and B) reporter strains argue for a defect in SHH signaling in the progenitor niche of the DPW as the underlying molecular mechanism. Our model is consistent with the established role of LRP2 in promoting SHH signal reception in other embryonic tissues, such as the neuroepithelium (10). Hypothetically, we cannot exclude that LRP2 deficiency may also impact signaling pathways other than through SHH, although the nature of such pathways remains unknown.

The manifold cardiac phenotypes observed upon interception with the SHH pathway uncovered multiple roles for this morphogen in heart morphogenesis (51). Among other functions, SHH is necessary for arterial pole formation as loss of SHH signaling in *Shh*^−/− mice or in chick embryos treated with the SHH antagonist cyclopamine results in CAT formation (48,49). Conditional disruption of the SHH pathway mediator *Smoothened* (Smo) in Islet1-positive progenitor cells or a *Shh* conditional mutant using the *Nkx2.5*^cre deleter strain substantiated a role for SHH in OFT elongation and identified SHF progenitors as cell population receptive to SHH signals (35,54). Now, our findings identify LRP2 as an essential component of the SHH signaling machinery during OFT formation and implicate defects in SHH signaling in SHF progenitors of the DPW in CAT formation in receptor mutant mice. Using the *Gli1-CreER*^T2 reporter line, we showed an overall reduction in the number of SHH-responsive Islet1-positive progenitor cells in the *Lrp2*^−/− distal OFT tissue (Fig. 7A and C). Also, while these cells were mainly restricted to the DPW and the Tz in control hearts, they showed a more dispersed localization in the OFT tissue in mutants, overlapping with MF20 positive cardiac cells in Tz and OFT myocardium (Fig. 8A). In line with an impaired demarcation of DPW, Tz and OFT myocardium in *Lrp2*^−/− hearts, the expression domain for cardiac troponin I in mutants reached into the Tz, while E-cadherin expression, restricted to the Tz in controls, aberrantly extended more posteriorly into the DPW (Fig. 8C). Finally, the pattern of laminin, indicative of a more mature development of the basal lamina was restricted to the proximal regions of the Tz and the OFT myocardium in controls but extended into the distal Tz and anterior DPW in *Lrp2*^−/− heart tissue. Collectively, these findings support a role for LRP2 in establishing an SHH-dependent niche for cardiac progenitor cells in the DPW and in controlling their differentiation along a path to the OFT myocardium.

LRP2 likely acts as agonist for SHH signaling during OFT formation

In the LRP2 mutant OFT, both the number of Islet1-positive cells receptive to SHH signals but also the overall expression domain of Islet1-positive progenitor cells were reduced (Fig. 5). Thus, we cannot distinguish with certainty whether LRP2 deficiency primarily impacts SHH signaling in progenitor cells, thereby decreasing their numbers, or whether LRP2 is required for other aspects of cell maintenance and loss of SHH activity in this niche is a secondary consequence of progenitor cell loss. However, based on evidence provided in this study and in published work (10,11), an instructive role for LRP2 in facilitation SHH signaling in SHF progenitors seems likely.

The SHH signaling machinery is well characterized at the molecular level. In addition to the primary SHH receptor PTCH1, auxiliary SHH binding proteins are necessary to activate or inhibit the pathway in a context-dependent manner. This modulatory activity of SHH binding proteins has mainly been documented in the embryonic neuroepithelium (55,56), with

LRP2 being one of these essential SHH co-receptors. Dependent on the biological context, LRP2 may activate (by facilitating cell surface binding of the morphogen) (10) or inhibit (by directing SHH to lysosomal degradation) the SHH pathway (11). Data in here argue that during OFT formation, LRP2 acts as an agonist to promote the responsiveness of SHF progenitor cells to SHH cues. This hypothesis is supported by a recent study documenting a crucial role for SHH in activating progenitor gene expression and in inhibiting premature differentiation, thereby maintaining the progenitor cell population in the SHF (57). We also show that LRP2 ensures the proper migration pattern of SHH-responsive SHF progenitors during OFT elongation. These results are in line with findings that SHH-responsive progenitors from the anterior SHF migrate into the pulmonary vessel (58). Finally, a recent study on GATA4-regulated SHH signaling in cardiac progenitor cells documented the importance of SHH signals for SHF cell migration in mice (59). In this study, the migratory defect of *Gata4* haploinsufficient SHF progenitor cells was rescued by the over-activation of the hedgehog pathway using the constitutively activate Smo mutant *SmoM2*, reconstituting cell migration from the SHF into the OFT and ensuring proper OFT formation.

In conclusion, we uncovered a crucial role for LRP2 in maintenance of a pool of SHH-dependent progenitors in the anterior SHF, ensuring their differentiative fate as they migrate into the OFT tissue. These findings have identified a novel component of the SHH signaling machinery essential for OFT development and uncovered the molecular cause of conotruncal malformations in humans and mouse models lacking this receptor. Additional defects seen in LRP2-deficient hearts suggest that receptor activity may not be restricted to SHH-dependent progenitor cell fate specification during OFT formation but encompass other aspects of heart development, such as OFT cushion formation. The molecular mechanisms of LRP2 function in the later processes still require further elucidation.

Materials and Methods

Mouse models

Generation of mice with targeted *Lrp2* gene disruption has been described before (2). The *Lrp2* gene defect was analyzed in receptor-deficient and somite-matched littermates either wild-type (*Lrp2*^+/+) or heterozygous for the mutant *Lrp2* allele (*Lrp2*^+/−). Since heterozygous animals demonstrate no LRP2 haploinsufficiency phenotype, *Lrp2*^+/+ and *Lrp2*^+/− embryos were combined and referred to as control group in this study. Where indicated, the *Lrp2* deficient line was crossed with the *Gli1-CreER*^T2 (JAX; Stock 007913), the *Gli1_LacZ* (JAX; Stock 008211) or the *Tcf/Lef_LacZ* (Mohamed et al., 2004) reporter strains. Also, where applicable, the *Lrp2* deficient line was crossed with the *Wnt1-Cre* line (obtained from C. Birchmeier, Max-Delbrueck-Center, Berlin) and subsequently with the R26R (JAX; Stock 003474) reporter line to generate the *Wnt1-Cre_LacZ* reporter strain. All experiments involving animals were performed according to institutional guidelines following approval by local authorities (X9007/17).

Immunohistology

For hematoxylin and eosin (H + E) staining, embryos were fixed overnight in 4% paraformaldehyde in PBS at 4°C, followed by routine paraffin embedding and sectioning at 10 μm thickness. For lacZ or immunofluorescence stainings, embryos were fixed for 1–4 h in 4% paraformaldehyde in PBS at 4°C. Fixed embryos

were infiltrated with 30% sucrose in PBS overnight at 4°C, followed by 2 h incubation in 50% cryoprotectant Tissue-Tek® OCT in 30% sucrose, followed by 2 h incubation in 75% Tissue-Tek® OCT in 30% sucrose. Finally, the embryos were embedded in Tissue-Tek® OCT and subjected to 10 μm cryo-sectioning. For immunodetection of E-cadherin, PKC-ζ, cardiac troponin I or laminin, embryos were dehydrated and embedded in paraffin and sectioned at 10 μm.

Immunohistochemical analysis was carried out by incubation of tissue sections with primary antibodies at the following dilutions: guinea pig anti-LRP2 (1:2000; made in-house by immunizing guinea pigs with full-length LRP2 isolated from rabbit kidney), mouse anti-AP2α (1:50; DSHB; Santa Cruz), mouse anti-Islet1 (1:50; DSHB), goat anti-Nkx2.5 (1:100; Santa Cruz), rabbit anti-GFP (1:400; Abcam), mouse anti-MF20 (1:50; DSHB), rat anti-BrdU (1:100; AbD Serotec), mouse anti-E-cadherin (1:200; BD Transduction Laboratories), goat anti-cardiac troponin I (1:100; Abcam), rabbit anti-laminin (1:200; Sigma), rabbit anti-PKC-ζ (1:200; Sigma), rabbit anti-Arl13b (1:200; Proteintech), rat anti-CD31 (PECAM-1, 1:300; BD Pharmigen) and mouse anti-SMA (1:300; Sigma). Primary antibodies were visualized using secondary antisera conjugated with Alexa Fluor 488, 555 or 647 (1:500; Invitrogen and Jackson Immuno Research) or with Biotin-SP (1:100; Jackson Immuno Research) followed by fluorescent conjugates of streptavidin (1:500; Invitrogen). Image acquisitions were carried out using a Leica DMI 6000B inverted microscope or Leica SPE or Leica SP5 confocal microscopes.

In situ hybridization

ISH on paraffin sections was described earlier (60). Plasmids for digoxigenin (DIG)-labeled riboprobes were kindly provided by L. Robertson (University of Oxford, Oxford; *Bmp4*), E. Sock (Institute for Biochemistry, Erlangen; *Sox9*), W. Birchmeier (Max-Delbrueck-Center, Berlin; *Islet1, Tbx1*), C. Birchmeier (Max-Delbrueck-Center, Berlin; *Sox10*), R. Kelly (Aix Marseille Université, Marseille; *Sema3c*) and S. Meilhac (Imagine—Institut Pasteur, Paris; *Wnt11*).

Tamoxifen injection

Tamoxifen was prepared at 20 mg/ml in peanut butter oil. It was injected at a final dose of 2 mg into pregnant females at E7.5. Embryos were collected at E10.5 and fixed for 4 h, followed by cryo-sectioning and standard immunohistology using rabbit anti-GFP (1:400; Abcam) and mouse anti-Islet1 (1:50; DSHB) antibodies or guinea pig anti-LRP2 (1:2000; made in-house) and mouse anti-MF20 (1:50; DSHB) antibodies. The numbers of YFP positive and YFP/Islet1 double positive cells in the distal OFT vessel were counted on 5–9 coronal sections through the distal OFT vessel per embryo for a total of 6 control and 6 *Lrp2*$^{-/-}$ embryos. The number of YFP/MF20 double positive cells in the OFT was counted on 5–8 sagittal sections per embryo for a total of 5 control and 5 *Lrp2*$^{-/-}$ embryos.

Measurement of OFT length

The length of the OFT was measured by taking the mean derived from the lengths of the upper (green line) and lower (blue line) OFT walls from 5 sagittal sections per embryo for a total of 6 control and 7 *Lrp2*$^{-/-}$ E10.5 embryos using ImageJ.

Statistical analysis

Statistical significance was tested using the GraphPad Prism 7 software. Results comparing two groups were analyzed by Student's *t* test (Figs 7B, C, E and 8B). *P* values are indicated in the respective figure legends.

Supplementary Material

Supplementary Material is available at *HMG* online.

Acknowledgement

Funding

References

1. Willnow, T.E. and Christ, A. (2017) Endocytic receptor LRP2/megalin—of holoprosencephaly and renal Fanconi syndrome. *Pflugers Arch. - Eur. J. Physiol.*, **469**, 907–916.
2. Willnow, T.E., Hilpert, J., Armstrong, S.A. *et al.* (1996) Defective forebrain development in mice lacking gp330/megalin. *Proc. Natl. Acad. Sci. U. S. A.*, **93**, 8460–8464.
3. Spoelgen, R., Hammes, A., Anzenberger, U. *et al.* (2005) LRP2/megalin is required for patterning of the ventral telencephalon. *Development*, **132**, 405–414.
4. Storm, T., Heegaard, S., Christensen, E.I. *et al.* (2014) Megalin-deficiency causes high myopia, retinal pigment epithelium-macromelanosomes and abnormal development of the ciliary body in mice. *Cell Tissue Res.*, **358**, 99–107.
5. Cases, O., Joseph, A., Obry, A. *et al.* (2015) Foxg1-Cre mediated Lrp2 inactivation in the developing mouse neural retina, ciliary and retinal pigment epithelia models congenital high myopia. *PLoS One*, **10**, e0129518.
6. Kantarci, S., Al-Gazali, L., Hill, R.S. *et al.* (2007) Mutations in LRP2, which encodes the multiligand receptor megalin, cause Donnai-barrow and facio-oculo-acoustico-renal syndromes. *Nat. Genet.*, **39**, 957–959.
7. Kantarci, S., Ragge, N.K., Thomas, N.S. *et al.* (2008) Donnai-barrow syndrome (DBS/FOAR) in a child with a homozygous LRP2 mutation due to complete chromosome 2 paternal isodisomy. *Am. J. Med. Genet. A*, **146A**, 1842–1847.
8. Rosenfeld, J.A., Ballif, B.C., Martin, D.M. *et al.* (2010) Clinical characterization of individuals with deletions of genes in holoprosencephaly pathways by aCGH refines the phenotypic spectrum of HPE. *Hum. Genet.*
9. Schrauwen, I., Sommen, M., Claes, C. *et al.* (2014) Broadening the phenotype of LRP2 mutations: a new mutation in LRP2 causes a predominantly ocular phenotype suggestive of stickler syndrome. *Clin. Genet.*, **86**, 282–286.
10. Christ, A., Christa, A., Kur, E. *et al.* (2012) LRP2 is an auxiliary SHH receptor required to condition the forebrain ventral midline for inductive signals. *Dev. Cell*, **22**, 268–278.

11. Christ, A., Christa, A., Klippert, J. *et al*. (2015) LRP2 acts as SHH clearance receptor to protect the retinal margin from mitogenic stimuli. *Dev. Cell*, **35**, 36–48.

12. Cases, O., Perea-Gomez, A., Aguiar, D.P. *et al*. (2013) Cubilin, a high affinity receptor for fibroblast growth factor 8, is required for cell survival in the developing vertebrate head. *J. Biol. Chem.*, **288**, 16655–16670.

13. Zaidi, S., Choi, M., Wakimoto, H. *et al*. (2013) De novo mutations in histone-modifying genes in congenital heart disease. *Nature*, **498**, 220–223.

14. Li, Y., Klena, N.T., Gabriel, G.C. *et al*. (2015) Global genetic analysis in mice unveils central role for cilia in congenital heart disease. *Nature*, **521**, 520–524.

15. van der Linde, D., Konings, E.E.M., Slager, M.A. *et al*. (2011) Birth prevalence of congenital heart disease worldwide. *A systematic review and meta-analysis. J. Am. Coll. Cardiol.*, **58**, 2241–2247.

16. Baardman, M.E., Zwier, M.V., Wisse, L.J. *et al*. (2016) Common arterial trunk and ventricular non-compaction in Lrp2 knockout mice indicate a crucial role of LRP2 in cardiac development. *Dis. Model. Mech.*, **9**, 413–425.

17. Lincoln, J., Kist, R., Scherer, G. *et al*. (2007) Sox9 is required for precursor cell expansion and extracellular matrix organization during mouse heart valve development. *Dev. Biol.*, **305**, 120–132.

18. Snider, P., Olaopa, M., Firulli, A.B. *et al*. (2007) Cardiovascular development and the colonizing cardiac neural crest lineage. *Sci. World J.*, **7**, 1090–1113.

19. Waldo, K., Miyagawa-Tomita, S., Kumiski, D. *et al*. (1998) Cardiac neural crest cells provide new insight into Septation of the cardiac outflow tract: aortic sac to ventricular septal closure. *Dev. Biol.*, **196**, 129–144.

20. Claudio, C., Alexandre, F., De, B.C. *et al*. (2018) Epithelial properties of the second heart field. *Circ. Res.*, **122**, 142–154.

21. Assémat, E., Châtelet, F., Chandellier, J. *et al*. (2005) Overlapping expression patterns of the multiligand endocytic receptors cubilin and megalin in the CNS, sensory organs and developing epithelia of the rodent embryo. *Gene Expr. Patterns*, **6**, 69–78.

22. Fisher, C.E. and Howie, S.E.M. (2006) The role of megalin (LRP-2/Gp330) during development. *Dev. Biol.*, **296**, 279–297.

23. Jiang, X., Rowitch, D.H., Soriano, P. *et al*. (2000) Fate of the mammalian cardiac neural crest. *Development*, **127**, 1607–1616.

24. Buckingham, M., Meilhac, S. and Zaffran, S. (2005) Building the mammalian heart from two sources of myocardial cells. *Nat. Rev. Genet.*, **6**, 826.

25. Kodo, K., Shibata, S., Miyagawa-Tomita, S. *et al*. (2017) Regulation of Sema3c and the interaction between cardiac neural crest and second heart field during outflow tract development. *Sci. Rep.*, **7**, 6771.

26. Francou, A., Saint-Michel, E., Mesbah, K. *et al*. (2014) TBX1 regulates epithelial polarity and dynamic basal filopodia in the second heart field. *Development*, **141**, 4320–4331.

27. Rochais, F., Mesbah, K. and Kelly, R.G. (2009) Signaling pathways controlling second heart field development. *Circ. Res.*, **104**, 933–942.

28. Lin, L., Cui, L., Zhou, W. *et al*. (2007) β-Catenin directly regulates Islet1 expression in cardiovascular progenitors and is required for multiple aspects of cardiogenesis. *PNAS*, **104**, 9313–9318.

29. Schleiffarth, J.R., Person, A.D., Martinsen, B.J. *et al*. (2007) Wnt5a is required for cardiac outflow tract Septation in mice. *Pediatr. Res.*, **61**, 386–391.

30. Zhou, W., Lin, L., Majumdar, A. *et al*. (2007) Modulation of morphogenesis by noncanonical Wnt signaling requires ATF/CREB family–mediated transcriptional activation of TGFβ2. *Nat. Genet.*, **39**, 1225–1234.

31. Phillips Helen, M., Murdoch Jennifer, N., Bill, C. *et al*. (2005) Vangl2 acts via RhoA Signaling to regulate polarized cell movements during development of the proximal outflow tract. *Circ. Res.*, **96**, 292–299.

32. Ramsbottom, S.A., Sharma, V., Rhee, H.J. *et al*. (2014) Vangl2-regulated polarisation of second heart field-derived cells is required for outflow tract lengthening during cardiac development. *PLoS Genet.*, **10**, e1004871.

33. Sinha, T., Wang, B., Evans, S. *et al*. (2012) Disheveled mediated planar cell polarity signaling is required in the second heart field lineage for outflow tract morphogenesis. *Dev. Biol.*, **370**, 135–144.

34. Prall, O.W.J., Menon, M.K., Solloway, M.J. *et al*. (2007) An Nkx2-5/Bmp2/Smad1 negative feedback loop controls heart progenitor specification and proliferation. *Cell*, **128**, 947–959.

35. Goddeeris, M.M., Schwartz, R., Klingensmith, J. *et al*. (2007) Independent requirements for hedgehog signaling by both the anterior heart field and neural crest cells for outflow tract development. *Development*, **134**, 1593–1604.

36. Ihrie, R.A., Shah, J.K., Harwell, C.C. *et al*. (2011) Persistent sonic hedgehog signaling in adult brain determines neural stem cell positional identity. *Neuron*, **71**, 250–262.

37. Kelly, R.G. (2012) Chapter two - The second heart field. In Bruneau, B.G. (ed), *Current Topics in Developmental Biology. Heart Development*. Academic Press, Vol. 100, pp. 33–65.

38. Gibbs, B.C., Damerla, R.R., Vladar, E.K. *et al*. (2016) Prickle1 mutation causes planar cell polarity and directional cell migration defects associated with cardiac outflow tract anomalies and other structural birth defects. *Biology Open*, **5**, 323–335.

39. Soh, B.-S., Buac, K., Xu, H. *et al*. (2014) N-cadherin prevents the premature differentiation of anterior heart field progenitors in the pharyngeal mesodermal microenvironment. *Cell Res.*, **24**, 1420–1432.

40. Xia, M., Luo, W., Jin, H. *et al*. (2019) HAND2-mediated epithelial maintenance and integrity in cardiac outflow tract morphogenesis. *Development*, 146.

41. Suzuki, A. (2006) The PAR-aPKC system: lessons in polarity. *J. Cell Sci.*, **119**, 979–987.

42. Eley, L., Alqahtani, A.M., MacGrogan, D. *et al*. (2018) A novel source of arterial valve cells linked to bicuspid aortic valve without raphe in mice. *Elife*, **7**.

43. Francou, A., Saint-Michel, E., Mesbah, K. *et al*. (2013) Second heart field cardiac progenitor cells in the early mouse embryo. *Biochim. Biophys. Acta*, **1833**, 795–798.

44. Dyer, L.A. and Kirby, M.L. (2009) The role of secondary heart field in cardiac development. *Dev. Biol.*, **336**, 137–144.

45. Kwon, C., Arnold, J., Hsiao, E.C. *et al*. (2007) Canonical Wnt signaling is a positive regulator of mammalian cardiac progenitors. *PNAS*, **104**, 10894–10899.

46. Cohen, E.D., Wang, Z., Lepore, J.J. *et al*. (2007) Wnt/beta-catenin signaling promotes expansion of Isl-1-positive cardiac progenitor cells through regulation of FGF signaling. *J. Clin. Invest.*, **117**, 1794–1804.

47. Ai, D., Fu, X., Wang, J. *et al*. (2007) Canonical Wnt signaling functions in second heart field to promote right ventricular growth. *PNAS*, **104**, 9319–9324.

48. Klaus, A., Saga, Y., Taketo, M.M. *et al*. (2007) Distinct roles of Wnt/β-catenin and bmp signaling during early cardiogenesis. *PNAS*, **104**, 18531–18536.

49. Yang, L., Cai, C.-L., Lin, L. *et al*. (2006) Isl1Cre reveals a common bmp pathway in heart and limb development. *Development*, **133**, 1575–1585.

50. Pandur, P., Läsche, M., Eisenberg, L.M. *et al*. (2002) Wnt-11 activation of a non-canonical Wnt signalling pathway is required for cardiogenesis. *Nature*, **418**, 636.

51. Wiegering, A., Rüther, U. and Gerhardt, C. (2017) The role of hedgehog signalling in the formation of the ventricular septum. *J. Dev. Biol*., **5**, 17.

52. Dyer, L.A. and Kirby, M.L. (2009) Sonic hedgehog maintains proliferation in secondary heart field progenitors and is required for normal arterial pole formation. *Dev. Biol*., **330**, 305–317.

53. Washington Smoak, I., Byrd, N.A., Abu-Issa, R. *et al*. (2005) Sonic hedgehog is required for cardiac outflow tract and neural crest cell development. *Dev. Biol*., **283**, 357–372.

54. Lin, L., Bu, L., Cai, C.-L. *et al*. (2006) Isl1 is upstream of sonic hedgehog in a pathway required for cardiac morphogenesis. *Dev. Biol*., **295**, 756–763.

55. Christ, A., Herzog, K. and Willnow, T.E. (2016) LRP2, an auxiliary receptor that controls sonic hedgehog signaling in development and disease. *Dev. Dyn*., **245**, 569–579.

56. Allen, B.L., Song, J.Y., Izzi, L. *et al*. (2011) Overlapping roles and collective requirement for the Coreceptors GAS1, CDO, and BOC in SHH pathway function. *Dev. Cell*, **20**, 775–787.

57. Rowton, M., Hoffmann, A.D., Steimle, J.D. *et al*. (2019) Hedgehog signaling controls progenitor differentiation timing. *bioRxiv*, 270751.

58. Hoffmann, A.D., Peterson, M.A., Friedland-Little, J.M. *et al*. (2009) Sonic hedgehog is required in pulmonary endoderm for atrial septation. *Development*, **136**, 1761–1770.

59. Liu, J., Cheng, H., Xiang, M. *et al*. (2019) Gata4 regulates hedgehog signaling and Gata6 expression for outflow tract development. *PLoS Genet*., **15**, e1007711.

60. Jensen, A.M. and Wallace, V.A. (1997) Expression of sonic hedgehog and its putative role as a precursor cell mitogen in the developing mouse retina. *Development*, **124**, 363–371.